Energy-Efficient Blind Receiver-End Phase Synchronization for Collaborative Transmission over Nakagami-m Fading Channels

Smriti Sachdev and Swades De

Abstract

In collaborative wireless transmission from N independent nodes, up to N^2 power gain with respect to a single-node transmission is achievable at the receiver. However, achieving synchronization among the participating nodes can be energy-intensive due to high communication and computation overheads. To achieve distributed beamforming (DBF)-like N^2 power gains in resource-constrained nodes, we propose blind receiver-end phase synchronization methods with minimal overheads. The reduced processing is achieved in two steps. First, we transform the N-dimensional hypercube search space for phase corrections of N nodes into N one-dimensional searches. Next, we exploit the unique phase distribution of the Nakagami-m fading channel between the transmitters and the receiver to reduce the search space to a finite set of values. Two complementary methods, namely, reduced search space (RSS) method and extended RSS (extRSS) method are proposed that offer energy-efficient solutions in diverse channel fading conditions. For tractable performance analysis of the proposed methods, two approximations are derived for the Nakagami-m phase distribution, respectively for $m > 1$ and $m \leq 1$, and closed-form expressions are obtained for the average power gain in the two cases. The numerical and simulation results demonstrate that extRSS achieves fading agnostic near-perfect average power gain for 12 search points per transmitter, while RSS achieves near-perfect average power gain for 4 search points per transmitter, under strong LOS conditions. Both proposed methods are shown to have significantly reduced computational and energy requirements compared to the closest competitive approaches in the literature.

Index Terms

Collaborative transmission, distributed beamforming, energy efficiency, fading channel, Nakagami-m phase distribution, blind receiver-end phase synchronization

S. Sachdev is with the Centre for Development of Telematics, New Delhi, and the Department of Electrical Engineering, IIT Delhi, New Delhi, India (e-mail: smriti.sachdev@ee.iitd.ac.in). S. De is with the Department of Electrical Engineering and Bharti School of Telecommunication, IIT Delhi, New Delhi, India (e-mail: swadesd@ee.iitd.ac.in).

I. INTRODUCTION

Signals from multiple independent transmitters located at different positions can be phase-aligned to achieve power gain at a desired receiver. With N collaborating transmitters sending the same signal, power can be achieved at the receiver up to N^2 times compared to a single-node transmission. This collaborative approach can be applied to wireless information transfer [1], [2], wireless power transfer [3], [4], as well as simultaneous wireless information and power transfer [5], [6]. Power gain at the receiver can be used to increase communication range, or to maintain the same received power at $\frac{1}{N}$th fraction of the transmit power, thus conserving energy.

Power gain of N^2 is achieved when signals from all transmitters are synchronized at the receiver in time, frequency, and phase. Without synchronization, received power fluctuates due to random constructive and destructive interference, resulting in an average power of N. Achieving synchronization in a distributed setup is quite challenging, because, unlike in classical beamforming, the transmitters do not have a common clock. This causes frequency and phase offsets among the transmitter signals. Since the transmitters are placed at different and often unknown locations, the signals arrive at the receiver with unknown phases depending on the distance between the individual transmitters and the receiver. Also, the channels between each transmitter and the receiver further contribute to dynamic phase offset among these signals.

Phase synchronization at the receiver via collaborative phase correction at the transmitters, called distributed beamforming (DBF), needs frequent inter-node communication and receiver feedback. Unlike mobile communication systems, wireless sensor networks (WSNs) are significantly constrained by the deployment scenarios wherein frequent signaling based synchronization can be prohibitive due to energy limitation. Alternatively, phase correction of the independent transmitted signals can be attempted at the receiver.Given the limited processing power of wireless sensor nodes, synchronization methods must be compatible with low-end processors and should rely on minimal computational load and minimize energy consumption while providing stable gain under practical channel fading conditions. This study focuses on receiver-end processing-based blind phase synchronization (without receiver feedback to the transmitters) and specifically targets scalable solutions in a wide variety of fading channel conditions.

A. Related work and motivation

Though phase synchronization among the collaborating nodes are studied well, energy and communication constraints are not sufficiently addressed. In [7], the transmitters apply random

phase shifts in each iteration based on one-bit feedback from the receiver. It requires at least $5N$ feedback to attain 75% of the ideal beamforming gain [8]. Deterministic schemes such as in [9] employ a predefined sequence of phase shifts at the transmitters and use quantized receiver feedback for the required phase corrections. The methods in [10], [11] considered receiver-coordinated channel estimation and prediction using Kalman filter and feedback to the transmitters. In [12], the signal at the receiver is supplemented by a relay that applies constructive filtering in baseband and carrier domains for adding relay's and transmitter's signals at the receiver. The carrier synchronization in [13] requires several rounds of coordination among the transmitters. In sequential training scheme [14], each transmitter need to send M different phases and the receiver sends feedback to each with the best phase shift. It requires MN slots and N feedback for near-ideal beamforming gain. The parallel training scheme in [14] based on random phase perturbations and receiver feedback was shown to have slower convergence than the sequential scheme. Continuous coordination among the transmitters is required in [15] for inter-node ranging, whereas the approach in [16] requires additional hardware.

Some works considered resource efficiency in DBF-based receiver-end phase synchronization. In [17], DBF was considered with unmanned vehicles as transmitters. Their paths and transmit powers were co-optimized for energy efficiency; however, it did not detail the synchronization method. An iterative algorithm involving convex optimization with multiple constraints was used in [18] to minimize power for DBF in multiple-input-multiple-output (MIMO) full-duplex relaying. Here, in each iteration intermediate values of the optimization parameters are exchanged among the participating nodes, which is energy intensive. The receiver's channel measurement feedback period was optimized in [19], wherein the receiver implements a bank of two-state Kalman filters for each transmitter to track and predict the channel states. Distributed over-the-air computation in [20] with multicast beamforming for fast distributed optimization incurs high computational and energy cost, with complexity $\mathcal{O}(N^3)$. The approach in [21] achieves precise near field beamforming via high accuracy inter-node ranging, but has $\mathcal{O}(N^3)$ complexity. The scheme in [22] offers a more energy-efficient receiver design using ultra-low-power backscatter feedback, but imposes coordination and computation overhead on the transmitters, requiring each to perform multiple trial transmissions, typically $6(N-1)$ for phase correction.

The methods in [20]–[22] assume quasi-static channels and do not explicitly correct for channel fading, thus limiting their robustness in dynamic environments. Additionally, the approach in [23] requires multiple training stations (typically 3 to 5) with known and well-separated bearings as

well as prior knowledge of the receiver direction. It relies on centralized offline optimization, which must be repeated if the geometry of the transmitters, receiver, or training stations changes. Moreover, it assumes line-of-sight (LoS) conditions and does not compensate for channel-induced phase shifts, thus reducing its effectiveness in channel fading scenarios.

The existing receiver-centric phase synchronization methods [24]–[26] do not require feedback to the transmitters. The method in [24] relies on chance synchronization of the received signals that achieves a low rate of coherence. The approach in [25] requires the transmitters to send N times with predetermined phase shift, to enable the receiver to extract and weigh the signals for power gain. This method is unstable in fading channels and has high ($\mathcal{O}(N^3)$) processing overhead. The work in [26] improved upon the approach in [25] and achieved synchronization using N orthogonal transmissions, which also demonstrated energy efficiency over the competitive feedback-based (DBF) approach [14]. However, the method in [26] involves an exhaustive search across the search space with the computational load increasing linearly with N; this also impacts the processing-related energy consumption. Such receiver-end processing overhead may be infeasible for the lightweight energy-constrained nodes, thus limiting its scalability. This method also does not offer any optimization based on channel phase distribution statistics.

B. Contributions and scope of application

As an advance, this paper presents two complementary energy-efficient receiver-end phase synchronization, called reduced search space (RSS) method and extended RSS (extRSS) method, that achieve a similar power gain as in DBF in diverse fading conditions. These methods are blind, i.e., do not require inter-node communication or feedback, and exploit the unique properties of the Nakagami-m fading channel phase distribution for reducing the phase correction search space. These methods achieve high and stable power gain at the receiver while significantly saving on processing and energy cost. The key contributions and significance are as follows:

1) Efficient receiver-end blind phase synchronization methods RSS and extRSS are proposed, wherein the phase correction search space is simplified from N-dimensional hypercube to N one-dimensional lines. The search space is further reduced significantly irrespective of the fading parameter m by exploiting the nonuniformity of channel phase distribution in strong LOS conditions; *this unique feature has not been exploited in the literature so far.*
2) Closed-form expressions on power gain are derived analytically for the cases of $m > 1$ and $m \leq 1$ by approximating Nakagami-m phase distribution as Gaussian mixture and uniform,

respectively. *To the best of our knowledge such approximations are not available in the literature.* The accuracy of the approximations are verified through simulations.

3) The power gain of the RSS method is close to near-perfect DBF in strong LOS ($m \gg 1$); it also offers good gain even in severe fading conditions. Further, extRSS achieves fading-robust (m-independent) near-perfect power gain by trading off additional search points.
4) Receiver-end processing overhead in the proposed methods is shown to be significantly reduced with the reduced search space, making the proposed RSS and extRSS methods significantly energy-efficient compared to the available closest competitive approaches.

The proposed methods are energy-efficient, useful for achieving DBF-like power gains when receiving signals at energy-constrained nodes from multiple distributed sources. They provide power gain without receiver feedback (in absence of transmission capability or a feedback link) or where feedback is difficult (due to energy constraint at the receiver or unreliable feedback path). Such methods would especially facilitate ad hoc WSNs in various practical applications such as environmental monitoring, battlefield surveillance, disaster relief, and emergency response that are often constrained by harsh deployment environments, limited infrastructure, low-cost battery-powered devices, and rapidly changing channel conditions. The methods can also be used in cell-free MIMO networks with energy constraints, where distributed low-power nodes must cooperate efficiently without relying on extensive feedback or centralized coordination.

C. Paper organization

The paper is organized as follows: System model is discussed in Section II. The proposed phase synchronization procedure by search space dimensionality reduction is presented in Section III. Section IV presents the search space reduction method based on Nakagami-m phase distribution. Performance analysis of the proposed lightweight receiver-end phase synchronization is presented in Section V. Section VI contains the performance results. Section VII concludes the paper.

II. System Model

The system, in Fig. 1, consists of N independent wireless transmitters and one receiver. The nodes have independent clocks and associated random drifts. They are placed at locations unknown to each other and experience independent channel fading. As common in WSNs, the nodes are processing and energy constrained. The transmitters can individually reach the receiver, however, receiver feedback to transmitters is impossible or difficult due to its energy constraint.

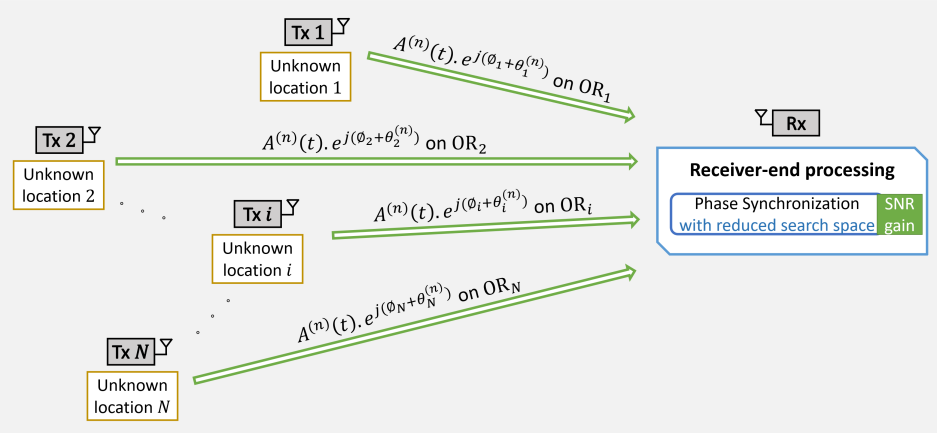

Fig. 1: System model for receiver-end phase synchronization. $A^{(n)}(t)$ is the common message from all transmitters in the nth communication cycle; OR_i and ϕ_i are respectively the ith transmitter's orthogonal resource and local oscillator initial phase offset; $\theta_i^{(n)}$ is the phase offset due to fading ith transmitter-to-receiver channel.

The transmitters collaborate to send common message $A^{(n)}(t)$ (shared amongst the nodes out of band) to the receiver, where superscript n represents the nth communication cycle. Each transmitter utilizes an orthogonal resources OR_i to transmit the common message $A^{(n)}(t)$.

It is assumed that all the nodes are frequency and time synchronized by methods known in the literature. However, phase de-synchronization from various sources exists among the nodes. The local oscillator of each transmitter i introduces an independent phase shift ϕ_i to the signal. ϕ_i is considered uniformly distributed in $[-\pi, \pi)$. The channel between the transmitters and the receiver introduce independent phase shifts θ_i due to small-scale fading. The channel fading is modeled as a Nakagami-m distributed as it covers a wide range of fading severity and LOS strength. The impact of shadowing on signal phase during transmission is considered negligible. Further, it is assumed that the receiver front-end is able to mitigate the impact of frequency-selective channels through equalization or other known methods in the literature.

Instead of feedback to the transmitters, in the proposed methods the receiver computes to phase synchronize the transmitted signals which can result in up to N^2 power gain compared to the transmission from a single transmitter. The efficacy of these methods is measured by normalized power gain, which is the ratio of the realized gain to the ideal gain (N^2) under perfect synchronization. The energy efficiency of these methods is evaluated in terms of a reduction in the energy consumption in receiver-end processing compared to the competitive approaches.

The increased power at the receiver can be useful for higher data rate communication or lowering transmit power while maintaining the data rate. With sufficient power at the receiver for sending intermittent broadcast feedback to the transmitters, the phase corrections can be

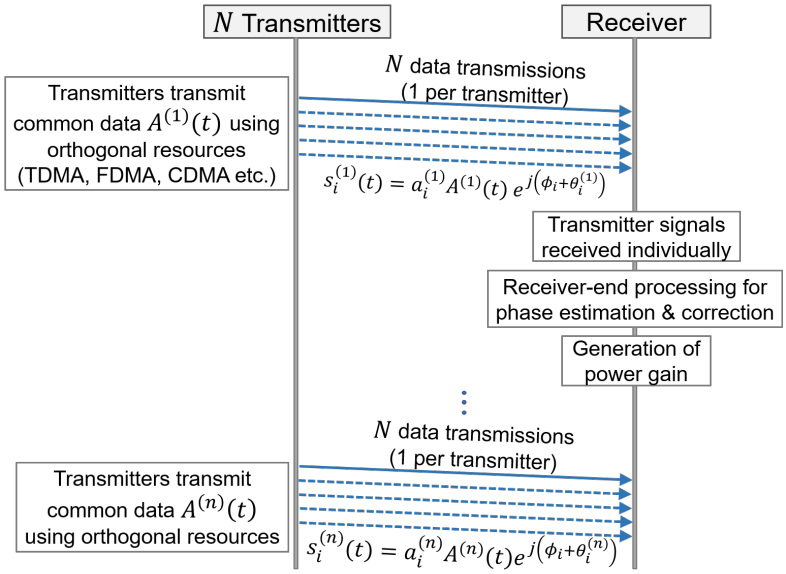

Fig. 2: Phase synchronization process, with signal $s_i^{(n)}(t)$ received from the ith transmitter having message $A^{(n)}(t)$, affected by channel gain $a_i^{(n)}$ and phase $\theta_i^{(n)}$ along with initial LO phase offset ϕ_i in nth communication cycle.

subsequently done at the transmitter, to form a beam over the air. This beamforming can also be utilized for efficient wireless power transfer [26] apart from information transfer.

The proposed phase synchronization procedure is elaborated in the subsequent sections.

III. Phase Synchronization Procedure

This section describes the proposed phase synchronization with minimized interaction among the participating nodes for energy efficiency. The procedure for achieving power gain consists of the following key steps: communication protocol and receiver-end processing, as detailed below.

A. Communication protocol

The transmitters transmit (a common message) in an orthogonal multi-access fashion, such as using TDMA, FDMA, OFDMA, or CDMA. The chosen protocol would depend on the existing technology support in the wireless network. This also ensures that no extra bandwidth provisioning is needed for phase synchronization beyond the existing allocation. The transmission matrix is shown in (1). For example, in TDMA, transmitter i, $i \in \{1, \cdots, N\}$, sends in slot i.

$$T_N = \begin{bmatrix} 1 & 0 & \dots & 0 \\ 0 & 1 & \dots & 0 \\ \vdots & \vdots & \ddots & \vdots \\ 0 & 0 & \dots & 1 \end{bmatrix} \triangleq I_N. \tag{1}$$

Each transmitter is required to make only one transmission per communication cycle similar to one-to-one communication. Also, pilot signals preceding the message are not required.

Let $\tilde{p_i}^{(n)}(t) = \Re\{p_i^{(n)}(t)e^{j2\pi f_{c_i}t}\}, i \in \{1, \cdots, N\}$, be the ith transmitter's signal in the nth message, where f_{c_i} is the carrier frequency, and $p_i^{(n)}(t)$ is the complex low-pass equivalent signal given by $p_i^{(n)}(t) = A^{(n)}(t)e^{j\phi_i}$. $A^{(n)}(t)$ is the message to be transferred and ϕ_i is the initial phase offset of the ith transmitter. At the receiver, the orthogonal signal received from the ith transmitter after passing through the channel $h_i^{(n)} = a_i^{(n)}e^{j\theta_i^{(n)}}$ is of the form

$$\tilde{r_i}(t) = \Re\Big\{h_i^{(n)}p_i^{(n)}e^{j2\pi f_{c_i}t} + w^{(n)}\Big\} = \Re\Big\{a_i^{(n)}A^{(n)}(t)e^{j(2\pi f_{c_i}t+\phi_i+\theta_i^{(n)})} + w^{(n)}\Big\} \tag{2}$$

where $a_i^{(n)} = \Big|h_i^{(n)}\Big|$, $\theta_i^{(n)} = \angle h_i^{(n)}$ and $w^{(n)}$ is the additive white Gaussian noise (AWGN) at the receiver. The receiver down-converts the signals to extract their complex low pass equivalents:

$$s_i^{(n)}(t) = a_i^{(n)}A^{(n)}(t)e^{j(\phi_i+\theta_i^{(n)})} + \hat{w}^{(n)}, \quad i \in \{1, \cdots, N\} \tag{3}$$

where $\hat{w}^{(n)}$ is the complex low pass equivalent of the AWGN.

This orthogonal transmission is followed by receiver-end processing to achieve power gain without any feedback to the transmitters or pilot signals. Hence, the proposed approach has no additional communication overhead compared to traditional one-to-one communication.

B. Receiver-end processing

As observed in (3), the received signals from the transmitters contain the accumulated error from the different sources. Thus, a single estimation/correction per transmitter signal is sufficient to correct all phase errors. Based on the collected transmitter signals, the receiver estimates the optimal phase correction for each transmitter signal individually through receiver-end processing.

1) Original optimization problem: For computing the optimal phase corrections $\alpha_i^{(n)}$ for each transmitter signal, the following optimization problem needs to be solved at the receiver:

$$\textbf{(P1)} : \{\alpha_1^{(n)}, \cdots, \alpha_N^{(n)}\} = \underset{\{z_1,\cdots,z_N\}}{arg\,max} \left|\sum_{i=1}^{N} s_i^{(n)}(t)e^{jz_i}\right|^2 \tag{4}$$

$$\text{s. t. } \textbf{(C1)} : 0 \leq z_i < 2\pi \quad \forall i \in \{1, \cdots, N\}.$$

(C1) defines the phase correction *search space*, which is an N-dimensional hypercube of side 2π. Solving the objective function for different $\{z_i\}$ values is processing intensive. An alternative is presented to reduce the processing by reducing the optimization problem to one dimension.

2) Dimensionality reduction: The *search space* in (4) is large and increases with N. We show that the N dimensional search space of size $(2\pi)^N$ can be reduced to N one-dimensional searches of size $2\pi N$ without affecting the optimality of solution. For this, we rewrite (4) as

$$\textbf{(P1)} : \underset{\{z_1,\cdots,z_N\}}{arg\,max} \left| \sum_{i=1}^{N} s_i^{(n)}(t) e^{jz_i} \right|^2 = \underset{\{z_1,\cdots,z_N\}}{arg\,max} \left| \sum_{i=1}^{N} a_i^{(n)} A^{(n)}(t) e^{j(\phi_i+\theta_i^{(n)}+z_i)} \right|^2 \tag{5}$$

$$\text{s. t. } \textbf{(C1)} : 0 \leq z_i < 2\pi \quad \forall i \in \{1, \cdots, N\},$$

Here, consistent with the basic consideration that each orthogonal transmission from the individual transmitters is detectable for the relative phase estimation and the subsequent receiver-end phase synchronization, the noise term is omitted for analytical tractability by assuming that the noise level is appreciably lower than the signal level of the individual orthogonal signals at the receiver[1]. Thus, in (5), $a_i^{(n)} A^{(n)}(t)$ can be safely ignored because $A^{(n)}(t)$ is a common term and $a_i^{(n)}$ does not impact in phase synchronization. However, the optimization cannot be solved numerically because $\phi_i + \theta_i^{(n)}$ is unknown. Now, we convert (P1) to a one-dimensional problem.

Proposition 1: A global optimal solution of (4) can be achieved by conducting N one-dimensional searches of the form

$$\phi_i + \theta_i + \alpha_i = \phi_0, \qquad \forall i \in \{1, \cdots, N\} \tag{6}$$

instead of searching the original search space spanning an N-dimensional hypercube of side 2π. $\phi_0 \in [0, 2\pi)$ is any arbitrary phase value which does not affect the optimality of the solution. Here, superscript (n) is dropped for simplicity of notation.

Proof: See Appendix A.

The equations in (6) indicate that the optimal value of phase correction is given by

$$\alpha_i = \phi_0 - (\phi_i + \theta_i). \tag{7}$$

However, solving the individual equations from (6) is non-trivial, as transmitter clock phase ϕ_i and channel phase θ_i are not known and difficult to measure. To proceed with finding the optimal phase correction α_i, we use the following corollary to Proposition 1:

[1]The receiver input $s_i^{(n)}(t)$ in (3) has two components: signal $a_i^{(n)} A^{(n)}(t) e^{j(\phi_i+\theta_i^{(n)})} \triangleq pe^{jq}$ and AWGN $\hat{w}^{(n)} \triangleq ce^{jd}$. The signal phase is $arg(s_i^{(n)}(t)) = \arctan\left(\frac{p\sin q + c\sin d}{p\cos q + c\cos d}\right) = \arctan\left(\frac{\sin q + \frac{c}{p}\sin d}{\cos q + \frac{c}{p}\cos d}\right) = \arctan\left(\frac{\sin q + \sqrt{SNR^{-1}}\sin d}{\cos q + \sqrt{SNR^{-1}}\cos d}\right)$. At high $SNR \triangleq \frac{p^2}{c^2}$, i.e., $p \gg c$, we have $arg(s_i^{(n)}(t)) \approx q$. Thus, the phase of the received signal and the accuracy of the phase synchronization are not significantly impacted by AWGN, as is typically prevalent in short-range wireless communications.

Algorithm 1: Finding optimal $\alpha_i^{(n)}$ as per proposed phase synchronization procedure

Input: $s_0^{(n)}(t), s_i^{(n)}(t), \Delta$

Output: α_i

Initialize: $\alpha_i = 0$, $maxPower = 0$;

for $y_i = 0$ *to* 2π *step* Δ **do**

  Compute $\left|s_0^{(n)}(t) + s_i^{(n)}(t)e^{jy_i}\right|^2$;

  if $\left|s_0^{(n)}(t) + s_i^{(n)}(t)e^{jy_i}\right|^2 > maxPower$ **then**

    $maxPower = \left|s_0^{(n)}(t) + s_i^{(n)}(t)e^{jy_i}\right|^2$;

    $\alpha_i = y_i$;

  end

end

Corollary: $\phi_i + \theta_i + \alpha_i = \phi_0$ is an optimal solution of

$$\textbf{(P2)} : \alpha_i = \underset{y_i}{arg\,max} \left|e^{j\phi_0} + e^{j(\phi_i+\theta_i+y_i)}\right|^2 \tag{8}$$

$$\text{s. t. } \textbf{(C2)} : 0 \leq \alpha_i < 2\pi$$

Proof: See Appendix B.

The objective function in (P2) cannot be computed numerically due to the lack of knowledge of $\phi_i + \theta_i$. Hence, we propose an algorithmic alternative based on the physical signals $s_i^{(n)}(t)$ received individually through the designed communication protocol presented in Section III-A.

3) Algorithmic Implementation: For a practical implementation based on the insights of Proposition 1 and its corollary, we define the receiver-end *pairwise phase synchronization algorithm* to find the optimal phase correction for each transmitter signal. The optimization problem of (8) is solved using Algorithm 1 by pairing each transmitter signal with a receiver reference signal $s_0^{(n)}(t)$ where $s_0^{(n)}(t)$ is a signal equivalent to $s_i^{(n)}(t)$ having phase ϕ_0 and can be one of the transmitter signals as well. $s_i^{(n)}(t)$ is phase shifted by all possible values from 0 to 2π with a selected step size of Δ and added to this reference signal. The resulting signal strength is evaluated in each step. Optimal phase correction is the phase shift that results in the maximum combined signal strength for the signal pair. This is repeated for each of the N signals.

C. Generation of power gain

The receiver shifts the phase of each of the collected transmitter signals according to the phase corrections computed in Section III-B above. Subsequently, the phase-synchronized signals are

added together to achieve the power gain. The final signal at the receiver can be expressed as

$$\sum_{i=1}^{N} s_i e^{j\alpha_i} = A(t) \sum_{i=1}^{N} e^{j(\phi_i+\theta_i+\alpha_i)}. \tag{9}$$

In the subsequent sections, through analysis and simulations, it is shown that the proposed phase synchronization procedures (even with further reduction in search space) achieve DBF-like power gains. It may be noted that the power gain is directly achieved at the receiver without any feedback overhead. This procedure can be repeated for subsequent communication cycles, thus offering continuous tracking of channel phase offsets and robustness to fast fading. Additionally, in a highly correlated channel with reasonable coherence time the synchronization requirements can be reduced further through intermittent receiver feedback as follows: the phase correction estimates calculated by the receiver can be sent back to the transmitters. The transmitters would correct their respective phases, followed by transmission on overlapping resources instead of orthogonal resources. This would enable synchronized data transmission with power gain achieved at the receiver antenna itself without the need for receiver-end processing. Once the channel decorrelates, the phase estimates would become outdated, resulting in a decrease in power gain at the receiver. At that point, the proposed RSS or extRSS process can be repeated to obtain the new phase estimates for the transmitters in the next transmission cycle.

In the next section, we show that the search space for the optimal phase corrections $\{\alpha_i\}$ can be significantly reduced by exploiting the channel phase distribution characteristics.

Remark 1. *As shown in Section III-B and III-C, the phase synchronization can be done through pairwise synchronization of the transmitted signals at the receiver. This insight inspired the design of orthogonal transmission in the communication protocol as presented in Section III-A.*

IV. Nakagami-m Phase Distribution based Search Space Reduction

Channel phase distribution is commonly considered as uniform, which corresponds to Rayleigh fading envelope, when there is no strong LOS. However, in practice, especially in short-range communications, in radiative wireless power transfer, or in fixed backhaul communication links, LOS component can be dominant [27], [28]. To account for a more generalized fading scenario, this work considers Nakagami-m channel phase distribution, with the m parameter varying from 0.5 (severe scattering) to 1 (Rayleigh) and further to a large value (Rician (strong LOS)).

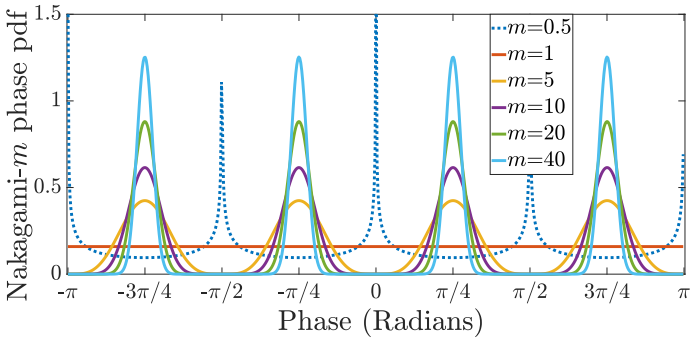

Fig. 3: Nakagami-m phase distribution pdf for different values of m.

Though Nakagami-m fading has been widely studied, most of these works focus on the channel envelope characteristics [29]–[34]. A few works have studied the channel phase [35]–[37]. These models are shown to have similar envelope and phase as the Hoyt and Rice distributions at limiting values of the parameters. An important observation from the models is that, contrary to common assumption, the channel phase is nonuniform for non-Rayleigh envelope, i.e., for all $m \neq 1$. The study in [38] has also validated this nonuniform nature using field measurements. Our proposed reduced search space methods exploit this nonuniformity in channel phase distribution.

In the following subsections, we first discuss the nature of the Nakagami-m phase distribution and then present the proposed search space reduction methods.

A. Nakagami-m phase distribution

The probability density function (pdf) of Nakagami-m phase distribution ($m \geq 0.5$) [35] is

$$p_\theta(\theta) = \frac{\Gamma(m)|\sin(2\theta)|^{m-1}}{2^m\Gamma^2(\frac{m}{2})}; \quad \theta \in [-\pi, \pi) \tag{10}$$

when the dominant energy component is equally distributed between the in-phase and quadrature components. Here, m signifies the fading severity; a large values of m represents less severe fading and stronger LOS conditions. Besides this model, two other mathematical models for Nakagami-m phase distribution have been discussed in [36] and [37], however, they also reduce to the phase model of [35] when the in-phase and quadrature components have equal energy.

The Nakagami-m phase distribution in (10) is plotted in Fig. 3. From [35], the phase distribution is nonuniform for all cases except $m = 1$ (Rayleigh envelope). Also, four high probability areas are observed in the form of sharp peaks for large values of m (strong LOS) with the peaks getting sharper as m increases. The peaks are located at $-\frac{3\pi}{4}, -\frac{\pi}{4}, \frac{\pi}{4}$, and $\frac{3\pi}{4}$ for all values of $m > 1$. However, when $m < 1$, the probability peaks are at phase values $-\pi, -\frac{\pi}{2}, 0$, and $\frac{\pi}{2}$.

Algorithm 2: Finding optimal α_i with proposed reduced search space

Input: $s_0^{(n)}(t), s_i^{(n)}(t), \alpha_i^{(1)}, \mathcal{J}$

Output: $\alpha_i^{(n)}$

Initialize: $y_i = 0, maxPower = 0$;

for *each* $y_i \in \mathcal{J}$ **do**

  Compute $\left|s_0^{(n)}(t) + s_i^{(n)}(t)e^{jy_i}\right|^2$;

  if $\left|s_0^{(n)}(t) + s_i^{(n)}(t)e^{jy_i}\right|^2 > maxPower$ **then**

    $maxPower = \left|s_0^{(n)}(t) + s_i^{(n)}(t)e^{jy_i}\right|^2$;

    $\tau_i^{(n)} = y_i$;

  end

end

$\alpha_i^{(n)} = \alpha_i^{(1)} + \tau_i^{(n)}$

B. Proposed reduced search space (RSS) method under strong LOS conditions ($m > 1$)

As discussed in the Section IV-A, for $m > 1$, Nakagami-m phase distribution is characterized by four high probability areas with sharp peaks; the peaks get sharper as m increases. For $m \gg 1$, these high probability areas tend to impulse functions at the location of the peaks, i.e., $-\frac{3\pi}{4}, -\frac{\pi}{4}, \frac{\pi}{4}$, and $\frac{3\pi}{4}$. We use this as a simplified approximation of the Nakagami-m phase distribution, with each impulse function weighted by $\frac{1}{4}$ to ensure a valid pdf. Mathematically,

$$p_\theta(\theta) = \frac{1}{4}\left\{\delta\left(\theta + \frac{3\pi}{4}\right) + \delta\left(\theta + \frac{\pi}{4}\right) + \delta\left(\theta - \frac{\pi}{4}\right) + \delta\left(\theta - \frac{3\pi}{4}\right)\right\}, \tag{11}$$

where $\theta \in [-\pi, \pi)$. Consider (7), which indicates the ideal phase correction value for the ith transmitter. Let a numeric superscript $^{(n)}$ indicate the nth subsequent communication cycle. Rewriting (7) for the nth communication cycle, we have,

$$\alpha_i^{(n)} = \phi_0 - (\phi_i + \theta_i^{(n)}) = \alpha_i^{(1)} - (\theta_i^{(n)} - \theta_i^{(1)}). \tag{12}$$

From (12), optimal $\alpha_i^{(n)}$ can be viewed as the difference of the optimal phase correction in the first communication cycle, $\alpha_i^{(1)}$, and the change in channel phase over subsequent communication cycles. It should be noted that the signals received from the transmitters contain the accumulated phase offsets. Thus, the exact values of channel phase shifts $\theta_i^{(1)}$and $\theta_i^{(n)}$ are not known and (12) cannot be directly solved for the optimal $\alpha_i^{(n)}$. However, $\alpha_i^{(1)}$ can be computed by scanning over

0 to 2π using the method in Section III-B. Also, $\theta_i^{(n)} - \theta_i^{(1)}$ can be reduced to a finite set based on the high probability areas of $p_\theta(\theta)$ using (11) as described below (shifting by 2π as required):

$$p_{\theta^{(n)}-\theta^{(1)}}(\theta) = p_\theta(\theta) \circledast p_\theta(\theta) = \frac{1}{4}\left\{\delta(\theta+\pi) + \delta\Big(\theta+\frac{\pi}{2}\Big) + \delta(\theta) + \delta\Big(\theta-\frac{\pi}{2}\Big)\right\} \tag{13}$$

where $\theta \in [-\pi, \pi)$ and $\circledast$ denotes circular convolution. Thus, the possible values of $\theta_i^{(n)} - \theta_i^{(1)}$ are approximately limited to the set $\mathcal{J}$:

$$\mathcal{J} = \left\{-\pi, -\frac{\pi}{2}, 0, \frac{\pi}{2}\right\}. \tag{14}$$

Let $\tau_i^{(n)} \in \mathcal{J}$ be the estimate of $\theta_i^{(n)} - \theta_i^{(1)}$ given by the proposed algorithms. Thus, from (12),

$$\alpha_i^{(n)} = \alpha_i^{(1)} - \tau_i^{(n)}. \tag{15}$$

From (15), the updated optimization problem (8) for estimating $\tau_i^{(n)}$ and consequently $\alpha_i^{(n)}$ is

$$\textbf{(P3)}: \tau_i^{(n)} = \arg\max_{y_i^{(n)}} \left| e^{j\phi_0} + e^{j(\phi_i + \theta_i^{(n)} + \alpha_i^{(1)} - y_i^{(n)})} \right|^2 \tag{16}$$

$$\text{s.t. } \textbf{(C3)}: y_i^{(n)} \in \mathcal{J}.$$

Thus, the search space for each pairwise phase synchronization, given in Section III-B, reduces to a set of four values given by $\mathcal{J}$. The objective function in (P3) cannot be computed numerically due to the lack of knowledge of ϕ_i and θ_i. Hence, we propose an algorithmic approach using the signals $s_i^{(n)}(t)$ received individually by the designed communication protocol.

To find the optimal phase corrections with reduced search space, we adopt the approach of Algorithm 2 similar to Algorithm 1 by using the physically received signals $s_i^{(n)}(t)$. For each pairwise phase synchronization, the algorithm identifies the phase from the reduced set, which results in maximum combined signal strength. The computed phase corrections are applied to the received signals, then they are added to achieve the power gain at the receiver. The performance results in Section VI will demonstrate the effectiveness of the reduced space search algorithm.

C. Proposed RSS for non-LOS conditions ($m \leq 1$)

In the following, we devise an RSS method for $m \leq 1$. As observed from Fig. 3, the high probability areas are more diffused for $m \leq 1$. Hence, the RSS method devised for LOS conditions $(m > 1)$ in Section IV-B is expected to give an inaccurate phase estimate for $m \leq 1$. Hence, we devise a modified RSS method that suits the channel phase distribution for $m \leq 1$.

Considering the high probability areas as weighted impulse functions as in Section IV-B, the approximated Nakagami-m phase pdf for $m \leq 1$ is:

$$p_\theta(\theta) = \frac{1}{4}\left\{\delta(\theta+\pi) + \delta\left(\theta+\frac{\pi}{2}\right) + \delta(\theta) + \delta\left(\theta-\frac{\pi}{2}\right)\right\}, \tag{17}$$

where $\theta \in [-\pi, \pi)$. Solving for $p_{\theta^{(n)}-\theta^{(1)}}(\theta)$ by using circular convolution we have,

$$p_{\theta^{(n)}-\theta^{(1)}}(\theta) = p_\theta(\theta) \circledast p_\theta(\theta) = \frac{1}{4}\left\{\delta(\theta+\pi) + \delta\left(\theta+\frac{\pi}{2}\right) + \delta(\theta) + \delta\left(\theta-\frac{\pi}{2}\right)\right\}, \tag{18}$$

$\theta \in [-\pi, \pi)$. Hence, based on the possible values of $\theta_i^{(n)} - \theta_i^{(1)}$, and using (15) and (16), the search space for pairwise phase synchronization for $m \leq 1$ also reduces to the set given in (14).

Remark 2. *The proposed method does not require the estimation of the parameter m for search space reduction, as the reduced search space is equivalent for $m > 1$ and $m \leq 1$ despite the difference in nature of the Nakagami-m phase distribution for these range of m values.*

D. Proposed extended RSS method (extRSS)

The RSS method significantly reduces the search space to only 4 values based on high-probability peaks in $p_{\theta^{(n)}-\theta^{(1)}}(\theta)$. The accuracy of phase correction therefore depends on a statistical phenomenon where θ is given by (10). Although less likely, the sample points of $\theta^{(n)} - \theta^{(1)}$ can sometimes lie away from the peaks, especially for lower values of m where the high probability areas are more diffused. This results in lower power gain at lower values of m.

We propose a complementary extended RSS method for improving the power gains at lower values of m at the cost of some marginally increased search overhead. The objective is to introduce a few judiciously chosen additional search points to limit the processing and energy costs. For this, one additional search point is introduced between the high probability peak and the low probability trough in $p_{\theta^{(n)}-\theta^{(1)}}(\theta)$. Let this point be at a distance K from the high probability peak. This strategy results in a total of 12 search points instead of 4, given by,

$$\mathcal{J} = \left\{-\pi, -\pi+K, -\frac{\pi}{2}-K, -\frac{\pi}{2}, -\frac{\pi}{2}+K, -K, 0, K, \frac{\pi}{2}-K, \frac{\pi}{2}, \frac{\pi}{2}+K, \pi-K\right\}. \tag{19}$$

This updated search space can then be applied to the optimization problem in (16) and the associated Algorithm 2, which results in further improved power gains at lower values of m.

V. Performance Analysis of Proposed Reduced Search Space Methods

In this section, we evaluate the performance of the proposed RSS and extRSS methods in terms of the achievable power gain at the receiver and energy/processing requirements.

A. Average received power gain

Denoting the corrected phase value of the ith transmitter's signal at the receiver in the nth communication cycle by $\Phi_i^{(n)}$,

$$\Phi_i^{(n)} = \phi_i + \theta_i^{(n)} + \alpha_i^{(n)} = \phi_i + \theta_i^{(n)} + \alpha_i^{(1)} - \tau_i^{(n)} \tag{20}$$

using (15), where $\tau_i^{(n)}$ is the proposed algorithm's estimate of $\theta_i^{(n)} - \theta_i^{(1)}$. The phase correction $\alpha_i^{(1)}$ is considered to be accurate and close to the theoretical value, as in the first communication cycle, the whole search space is searched exhaustively with a small step size instead of using a reduced search space. Thus, putting the theoretical value of $\alpha_i^{(1)}$ from (7) in (20), we have

$$\Phi_i^{(n)} = \phi_i + \theta_i^{(n)} + \phi_0 - (\phi_i + \theta_i^{(1)}) - \tau_i^{(n)} = \phi_0 + (\theta_i^{(n)} - \theta_i^{(1)}) - \tau_i^{(n)} = \phi_0 + X_i^{(n)} \tag{21}$$

where $X_i^{(n)} = (\theta_i^{(n)} - \theta_i^{(1)}) - \tau_i^{(n)}$ is the error in phase alignment between the phase corrected ith transmitter's signal at the receiver and the reference phase ϕ_0 in the proposed algorithm. To find the average power at the receiver, consider first the normalized power output at the receiver,

$$P_N = \frac{\left|\sum_{i=1}^{N} e^{j\Phi_i^{(n)}}\right|^2}{N} = \frac{\left|\sum_{i=1}^{N} e^{j(\phi_0 + X_i^{(n)})}\right|^2}{N} = \frac{\left|\sum_{i=1}^{N} e^{jX_i^{(n)}}\right|^2}{N} \tag{22}$$

by taking the common term $e^{j\phi_0}$ outside the summation, and using the identity $|ab| = |a|\,|b|$, a, $b \in \mathbb{C}$. The expected value of P_N using Proposition 2 of [39] is,

$$\mathbb{E}[P_N] = 1 + (N-1)(\mathbb{E}[\cos(X_i^{(n)})])^2. \tag{23}$$

Hence, the average power achieved at the receiver by the proposed algorithm is

$$\mathbb{E}[P] = N \times \mathbb{E}[P_N] = N[1 + (N-1)(\mathbb{E}[\cos(X_i^{(n)})])^2]. \tag{24}$$

Further, it is known that if $\mathbf{\Phi_X}(j\omega)$ is the characteristic function of X, then

$$\mathbb{E}[\cos(X)] = \Re(\mathbf{\Phi_X}(j\omega)) \quad \text{at} \quad \omega = 1, \quad \text{because} \tag{25}$$

$$\mathbf{\Phi_X}(j\omega) = \mathbb{E}[e^{j\omega X}] = \mathbb{E}[\cos(\omega X) + j\sin(\omega X)] = \mathbb{E}[\cos(\omega X)] + j\,\mathbb{E}[\sin(\omega X)]. \tag{26}$$

To proceed further, the distribution of $X_i^{(n)} = (\theta_i^{(n)} - \theta_i^{(1)}) - \tau_i^{(n)}$ is required. A few works in the literature [36], [40], [41] have discussed higher order statics of Nakagami-m phase distribution, however, the required distribution of $\theta_i^{(n)} - \theta_i^{(1)}$ has not been explored. Moreover, an exact analysis using the closed-form phase distribution expressions of [35]–[37] leads to complex formulations. Hence, we propose a tractable analytical approximations for the Nakagami-m phase distribution.

Since the nature of this distribution varies significantly for $m \leq 1$ and $m > 1$, the approximations are derived separately. Using these, the pdf and characteristic function of $X_i^{(n)}$ are evaluated and subsequently the expression for the achievable average power estimate is obtained.

1) ***Case 1:*** $m > 1$*:* The presence of multiple peaks in the Nakagami-m phase distribution for $m > 1$ motivates approximating each of the peaks with a Gaussian distribution.

Proposition 2: For large values of m, the Nakagami-m phase distribution can be approximated as a mixture of four Gaussian distributions. The approximate form is given by

$$p_\theta(\theta) = \frac{1}{4}\left[\mathcal{N}\left(\frac{-3\pi}{4},\, \sigma^2\right) + \mathcal{N}\left(\frac{-\pi}{4},\, \sigma^2\right) + \mathcal{N}\left(\frac{\pi}{4},\, \sigma^2\right) + \mathcal{N}\left(\frac{3\pi}{4},\, \sigma^2\right)\right], \tag{27}$$

where $\theta \in [-\pi, \pi)$, and $\sigma^2 = \frac{1}{4(m-1)}$ is the variance of the individual Gaussian distributions.

Proof: See Appendix C.

Now, consider the pdf of $\theta_i^{(n)} - \theta_i^{(1)}$, which is equivalent to the pdf of $\theta_i^{(n)} + \theta_i^{(1)}$, as $p_\theta(\theta)$ is symmetric about zero. Assuming $\theta_i^{(n)}$ and $\theta_i^{(1)}$ are independent, pdf of $\theta_i^{(n)} - \theta_i^{(1)}$ is:

$$\begin{aligned} p_{\theta^{(n)}-\theta^{(1)}}(\theta) &= p_\theta(\theta) \circledast p_\theta(\theta) \\ &= \frac{1}{4}\left[\mathcal{N}\left(-\pi,\, 2\sigma^2\right) + \mathcal{N}\left(-\frac{\pi}{2},\, 2\sigma^2\right) + \mathcal{N}\left(0,\, 2\sigma^2\right) + \mathcal{N}\left(\frac{\pi}{2},\, 2\sigma^2\right)\right], \quad \theta \in [-\pi, \pi) \end{aligned} \tag{28}$$

using $\mathcal{N}(\mu_a,\, \sigma^2) \circledast \mathcal{N}(\mu_b,\, \sigma^2) = \mathcal{N}(\mu_a + \mu_b,\, 2\sigma^2)$, and shifting by 2π where required. It can be noted from (28) that the pdf of $\theta_i^{(n)} - \theta_i^{(1)}$ is another mixture of four Gaussian distributions with variance $2\sigma^2$, and peaks or means $\mu_l, l = 1, \cdots, 4$ located at $-\pi, -\frac{\pi}{2}$, 0, and, $\frac{\pi}{2}$.

To derive the pdf of $X_i^{(n)} = (\theta_i^{(n)} - \theta_i^{(1)}) - \tau_i^{(n)}$ from the above, note that the value of $\tau_i^{(n)}$ is chosen by the proposed algorithm to minimize the error in phase alignment. For example, for any sample point $\theta_i^{(n)} - \theta_i^{(1)}$, the algorithm chooses that estimate from the reduced search space set $\mathcal{J}$ which is closest to the sample point. Thus, the selection zone for any search point in $\mathcal{J}$ extends from the mid-point between that search point and the preceding search point to the mid-point between that search point and the succeeding search point in the $\theta_i^{(n)} - \theta_i^{(1)}$ pdf (wrapping around by 2π where required). Each of these selection zones is composed of segments of the four Gaussians in (28)). Let the segment of the lth Gaussian in the selection zone of the kth search point $d_k, k = 1, 2, \cdots, D$ be denoted by $\mathcal{N}_{k,l}^t$, where t denotes that the Gaussian is truncated. The pdf of these truncated Gaussians can be represented mathematically as

$$\mathcal{N}_{k,l}^t \sim \mathcal{N}(\mu_l, 2\sigma^2), \quad \left[\frac{d_k + d_{k-1}}{2}, \frac{d_k + d_{k+1}}{2}\right] \tag{29}$$

Also, by phase wrapping, we have $d_{k-1} = d_D - 2\pi$ for $k = 1$ and $d_{k+1} = d_1 + 2\pi$ for $k = D$.

Furthermore, the subtraction of $\tau_i^{(n)}$ in $X_i^{(n)}$ results in the shifting of the Gaussian segments by $\tau_i^{(n)} = d_k$. The pdf of the shifted Gaussian segments is given by

$$\mathcal{N}_{k,l}^{t,s} \sim \mathcal{N}(\mu_l - d_k, 2\sigma^2), \quad \left[\frac{d_{k-1} - d_k}{2}, \frac{d_{k+1} - d_k}{2}\right]. \tag{30}$$

Hence, the pdf of $X_i^{(n)}$ is obtained by the superposition of these truncated and shifted Gaussians, with component weighted inversely proportional to the probability they carry. Mathematically,

$$p_X(x) = \frac{1}{4}\sum_{l=1}^{4}\sum_{k=1}^{D} w_{k,l}\mathcal{N}_{k,l}^{t,s} \tag{31}$$

where $x \in [-\pi, \pi)$ and $w_{k,l}$ represents the probability under the segment of Gaussian l with truncation limits determined by the search point k. For example, the probability under $\mathcal{N}(\mu, \sigma^2)$ in $[a, b)$ is given by $\frac{1}{2}\Big(\text{erf}\left(\frac{b-\mu}{\sqrt{2}\sigma}\right) - \text{erf}\left(\frac{a-\mu}{\sqrt{2}\sigma}\right)\Big)$. Now, the characteristic function of $X_i^{(n)}$ would be given by the weighted sum of the characteristic functions of $\mathcal{N}_{k,l}^{t,s}$.

Consider the characteristic function of a truncated Gaussian $\mathcal{N}(\mu, \Sigma^2)$, $[a, b]$ given by

$$\mathbf{\Phi_G}(j\omega) = e^{j\mu\omega - \Sigma^2\frac{\omega^2}{2}}\left[\frac{\varphi(\widetilde{\beta} - j\Sigma\omega) - \varphi(\widetilde{\alpha} - j\Sigma\omega)}{\varphi(\widetilde{\beta}) - \varphi(\widetilde{\alpha})}\right] \tag{32}$$

where $\widetilde{\alpha} = \frac{a-\mu}{\Sigma}, \widetilde{\beta} = \frac{b-\mu}{\Sigma}$, and $\varphi(k) = \frac{1}{2}\Big(1 + \text{erf}\,(\frac{k}{\sqrt{2}})\Big)$. Solving for the real part of (32),

$$\mathbf{\Phi_G}(j\omega) = \frac{e^{-\Sigma^2\frac{\omega^2}{2}}}{2(\varphi(\widetilde{\beta}) - \varphi(\widetilde{\alpha}))}\left[(\cos\mu\omega + j\sin\mu\omega) \times \left(\text{erf}\left(\frac{\widetilde{\beta} - j\Sigma\omega}{\sqrt{2}}\right) - \text{erf}\left(\frac{\widetilde{\alpha} - j\Sigma\omega}{\sqrt{2}}\right)\right)\right]. \tag{33}$$

Let $\text{erf}\left(\frac{\widetilde{\beta}-j\Sigma\omega}{\sqrt{2}}\right) = p(\omega) + jq(\omega)$ and $\text{erf}\left(\frac{\widetilde{\alpha}-j\Sigma\omega}{\sqrt{2}}\right) = r(\omega) + js(\omega)$ where,

$$p(\omega) = \Re\left\{\text{erf}\left(\frac{\widetilde{\beta} - j\Sigma\omega}{\sqrt{2}}\right)\right\} = \frac{1}{2}\left[\text{erf}\left(\frac{\widetilde{\beta} - j\Sigma\omega}{\sqrt{2}}\right) + \text{erf}\left(\frac{\widetilde{\beta} + j\Sigma\omega}{\sqrt{2}}\right)\right], \tag{34}$$

$$q(\omega) = \Im\left\{\text{erf}\left(\frac{\widetilde{\beta} - j\Sigma\omega}{\sqrt{2}}\right)\right\} = \frac{1}{2}\left[\text{erf}\left(\frac{\widetilde{\beta} - j\Sigma\omega}{\sqrt{2}}\right) - \text{erf}\left(\frac{\widetilde{\beta} + j\Sigma\omega}{\sqrt{2}}\right)\right], \tag{35}$$

$$r(\omega) = \Re\left\{\text{erf}\left(\frac{\widetilde{\alpha} - j\Sigma\omega}{\sqrt{2}}\right)\right\} = \frac{1}{2}\left[\text{erf}\left(\frac{\widetilde{\alpha} - j\Sigma\omega}{\sqrt{2}}\right) + \text{erf}\left(\frac{\widetilde{\alpha} + j\Sigma\omega}{\sqrt{2}}\right)\right], \tag{36}$$

$$s(\omega) = \Im\left\{\text{erf}\left(\frac{\widetilde{\alpha} - j\Sigma\omega}{\sqrt{2}}\right)\right\} = \frac{1}{2}\left[\text{erf}\left(\frac{\widetilde{\alpha} - j\Sigma\omega}{\sqrt{2}}\right) - \text{erf}\left(\frac{\widetilde{\alpha} + j\Sigma\omega}{\sqrt{2}}\right)\right]. \tag{37}$$

Then,

$$\mathbf{\Phi_G}(j\omega) = \frac{e^{-\Sigma^2\frac{\omega^2}{2}}(\cos\mu\omega + j\sin\mu\omega)}{2(\varphi(\widetilde{\beta}) - \varphi(\widetilde{\alpha}))}\Big[(p(\omega) - r(\omega)) + j(q(\omega) - s(\omega))\Big] \tag{38}$$

$$\implies \Re\Big\{\mathbf{\Phi_G}(j\omega)\Big\} = \frac{e^{-\Sigma^2\frac{\omega^2}{2}}}{2(\varphi(\widetilde{\beta}) - \varphi(\widetilde{\alpha}))}\Big[(p(\omega) - r(\omega))\cos\mu\omega - (q(\omega) - s(\omega))\sin\mu\omega\Big]. \tag{39}$$

Putting $\omega = 1$,

$$\Re\Big\{\boldsymbol{\Phi_G}(j\omega)\Big\}\Big|_{\omega=1} = \frac{e^{\frac{-\Sigma^2}{2}}}{2(\varphi(\widetilde{\beta}) - \varphi(\widetilde{\alpha}))}\Big[(p(1) - r(1))\cos\mu - (q(1) - s(1))\sin\mu\Big]. \tag{40}$$

Therefore,

$$\Re\{\boldsymbol{\Phi_X}(j\omega)\}\Big|_{\omega=1} = \frac{1}{4}\sum_{l=1}^{4}\sum_{k=1}^{D} w_{k,l}\Re\{\boldsymbol{\Phi}_{\boldsymbol{N}_{\boldsymbol{k,l}}^{\boldsymbol{t,s}}}}(j\omega)\}\Big|_{\omega=1}. \tag{41}$$

(41) can be evaluated for the proposed reduced search space method and its extended version.

Thus, the average power achieved at the receiver from (24), (25), and (41) is

$$\mathbb{E}[P] = N[1 + (N-1)(\Re\{\boldsymbol{\Phi_X}(j\omega)\}|_{\omega=1})^2]. \tag{42}$$

*2) **Case 2:** $m \leq 1$:* When $m = 1$, there are no peaks in the Nakagami-m phase distribution, as it takes the form of a uniform distribution. For $m < 1$, high probability peaks start to emerge, however, the area under the peaks remains negligible for m close to 1.

Proposition 3: For $m \to 1$, the Nakagami-m phase distribution can be approximated as a uniform distribution. The approximate form of the pdf is given by

$$p_\theta(\theta) \sim U[-\pi, \pi). \tag{43}$$

Proof: See Appendix D.

Based on (43), the pdf of $\theta_i^{(n)} - \theta_i^{(1)}$ is

$$p_{\theta^{(n)}-\theta^{(1)}}(\theta) \sim U[-\pi,\pi) \circledast U[-\pi,\pi) = U[-\pi,\pi). \tag{44}$$

To derive the pdf of $X_i^{(n)} = (\theta_i^{(n)} - \theta_i^{(1)}) - \tau_i^{(n)}$ from the above, note that the value of $\tau_i^{(n)}$ is chosen by the proposed algorithm to minimize the error in phase alignment. For example, for any sample point $\theta_i^{(n)} - \theta_i^{(1)}$, the algorithm chooses that $\tau_i^{(n)}$ from the set $\mathcal{J}$ which is closest to the sample point. Thus, the selection zone for any search point in $\mathcal{J}$ extends from the mid-point between that search point and the preceding search point to the mid-point between that search point and the succeeding search point in the $\theta_i^{(n)} - \theta_i^{(1)}$ pdf. Hence, the pdf of $\theta_i^{(n)} - \theta_i^{(1)}$ can be seen as constituting multiple uniform distribution segments. The number of such segments depends on the number of search points. Let $\{d_k\}, k = 1, 2, \cdots, D$ be the search points in set $\mathcal{J}$, then, each uniformly distributed segment around d_k can be denoted as

$$U_k \sim U\left[\frac{d_{k-1} + d_k}{2}, \frac{d_{k+1} + d_k}{2}\right). \tag{45}$$

Here, by using phase wrapping, $d_{k-1} = d_D - 2\pi$ for $k = 1$ and $d_{k+1} = d_1 + 2\pi$ for $k = D$. Furthermore, subtraction of $\tau_i^{(n)}$ in $X_i^{(n)}$ results in shifting of the uniformly distributed segments by $\tau_i^{(n)} = d_k$. Hence, the pdf of $X_i^{(n)}$ is formed by the superposition of shifted uniformly distributed segments denoted by U_k^s each weighted in proportion to the probability they carry (to maintain a valid pdf). The pdf of $X_i^{(n)}$ can be mathematically represented by

$$X_i^{(n)} \sim \sum_{k=1}^{D} w_k U_k^s = \sum_{k=1}^{D} w_k U\left[\frac{d_{k-1} - d_k}{2}, \frac{d_{k+1} - d_k}{2}\right) \tag{46}$$

where $w_k = \frac{d_{k+1} - d_{k-1}}{4\pi}$. Thus, the characteristic function of $X_i^{(n)}$ would be given by the weighted sum of the characteristic function of the individual uniformly distributed segments.

The characteristic function of uniform distribution, $U[a, b)$ is given by:

$$\boldsymbol{\Phi_U}(j\omega) = \mathbb{E}[e^{j\omega U}] = \begin{cases} \frac{e^{j\omega b} - e^{j\omega a}}{j\omega(b-a)} & \omega \neq 0 \\ 1 & \omega = 0. \end{cases} \tag{47}$$

$$\implies \Re\{\boldsymbol{\Phi_U}(j\omega)\}\Big|_{\omega=1} = \frac{\sin b - \sin a}{b - a} \tag{48}$$

Therefore, the characteristic function of $X_i^{(n)}$ evaluated at $\omega = 1$ is given by

$$\Re\{\boldsymbol{\Phi_X}(j\omega)\}\Big|_{\omega=1} = \sum_{k=1}^{D} w_k \Re\{\boldsymbol{\Phi_{U_k^s}}(j\omega)\}\Big|_{\omega=1} = \frac{1}{2\pi}\sum_{k=1}^{D}\Big\{\sin\Big(\frac{d_{k+1} - d_k}{2}\Big) - \sin\Big(\frac{d_{k-1} - d_k}{2}\Big)\Big\} \tag{49}$$

Equation (49) can be evaluated for the proposed reduced search space method and its extended version. Thus, the average power achieved at the receiver from (24), (25) and (49) is

$$\mathbb{E}[P] = N[1 + (N-1)(\Re\{\boldsymbol{\Phi_X}(j\omega)\}|_{\omega=1})^2]. \tag{50}$$

B. Processing requirements

The processing overhead is analyzed in terms of the number of clock cycles required to execute the proposed methods at the receiver. The clock cycles required in a microprocessor based system is related to the type and number of floating-point operations. We use CC3200 Texas Instruments Wireless MCU for Internet of Things applications powered by Arm Cortex-M4 MCU as a reference. This processor requires 1, 3, and 1 clock cycle, respectively, for real floating-point addition, multiplication, and comparison [42]. Table I shows the number of clock cycles required for the different steps in the proposed RSS and extRSS methods and that in the closest competitive approaches of [25] and [26]. A_q, M_q, and C_q denote the number of floating

point additions, multiplications, and total number of clock cycles respectively in step q of the different methods, with Arm Cortex M4 processor as reference. Also, U is the number of search points in the competitive approaches and $U_R = 4$ and $U_{eR} = 12$ are the number of search points in the proposed RSS and extRSS methods respectively after the search space reduction.

The total number of clock cycles indicates that the computational requirement in [25] increases $\mathcal{O}(N^3)$ with N, whereas the computations in the proposed RSS and extRSS methods increase linearly with N. Further, since the number of clock cycles is proportional to the number of search points, computations are significantly decreased by the proposed reduction in the search space compared to [26]. Through numerical plots in Section VI, it is also shown that despite a slight increase in search space in the proposed extRSS method as compared to the proposed RSS method, the computations are still significantly lower compared to the competitive approaches.

C. Energy consumption

Table I shows the analytical expressions derived for the energy consumption in processing E_p in the proposed methods and the closest competitive approaches. E_p is directly proportional to the total number of clock cycles required for processing and is given by $\frac{CVI}{f}$, where V is the operating voltage, I is the current consumption, and f is the operating frequency of the processor. Therefore, E_p is linear in N in the proposed RSS and extRSS methods, whereas it is $\mathcal{O}(N^3)$ for the method in [25]. Therefore, the approach in [25] has significantly higher energy consumption, especially when N increases. Further, as seen from Table I, E_p is also linearly dependent on the number of search points U or U_R or U_{eR}. Hence, the proposed RSS and extRSS methods reduce the energy consumption in processing by significantly reducing the search space to $U_R = 4$ in the proposed RSS method and $U_{eR} = 12$ in the proposed extRSS method. It may also be noted that the proposed methods and the closest competitive methods primarily rely on receiver-end processing for phase correction; they do not involve any transmitter-end processing.

It is noteworthy that the proposed RSS and extRSS methods significantly reduce the processing energy consumption without any additional communication overhead. Both the proposed methods and the method in [26] require $NE_{Tx}+NE_{Rx}$ Joules for synchronization between N transmitters and the receiver, where E_{Tx} and E_{Rx} are respectively the energy consumption in one wireless transmission and one wireless reception. In contrast, the receiver-end method in [25] requires $N^2E_{Tx} + NE_{Rx}$ energy for synchronization, which is much higher and increases as $\mathcal{O}(N^2)$.

TABLE I: Receiver-end processing requirements and energy consumption in the competitive methods

S.N.	Steps		Method in [25]	Method in [26]	Proposed RSS method	Proposed extRSS method
1	Transmission matrix inverse	A_1	$\frac{N^3}{6} - \frac{N^2}{2} + \frac{N}{3}$	0	0	0
		M_1	$\frac{N^3}{6} + \frac{N^2}{2} + \frac{N}{3}$	0	0	0
		C_1	$\frac{2N^3}{3} + N^2 + \frac{4N}{3}$	0	0	0
2	Individual signal extraction (Transmission matrix inverse $\times$ Received signal)	A_2	$N^2 - N$	0	0	0
		M_2	N^2	0	0	0
		C_2	$4N^2 - N$	0	0	0
3	Weighted addition $s' = s_0 + s_i e^{j\phi}$ where ϕ is changed from 0 to 2π in U or U_R or U_{eR} steps	A_3	$4U(N-1)$	$4UN$	$4U_RN$	$4U_{eR}N$
		M_3	$4U(N-1)$	$4UN$	$4U_RN$	$4U_{eR}N$
		C_3	$16U(N-1)$	$16UN$	$16U_RN$	$16U_{eR}N$
4	Magnitude of combined signal $\lvert s' \rvert^2$	A_4	$U(N-1)$	UN	U_RN	$U_{eR}N$
		M_4	$2U(N-1)$	$2UN$	$2U_RN$	$2U_{eR}N$
		C_4	$7U(N-1)$	$7UN$	$7U_RN$	$7U_{eR}N$
5	Comparison of combined signal strength	A_5	-	-	-	-
		M_5	-	-	-	-
		C_5	$(U-1)(N-1)$	$(U-1)N$	$(U_R-1)N$	$(U_{eR}-1)N$
6	Combining signals for power gain $s' = \sum_{i=1}^{N} s_i e^{j\phi_i}$	A_6	$4(N-1)$	$4N-2$	$4N-2$	$4N-2$
		M_6	$4(N-1)$	$4N$	$4N$	$4N$
		C_6	$16(N-1)$	$16N-2$	$16N-2$	$16N-2$
Total number of clock cycles, $C = \sum_{i=1}^{6} C_i$			$C^{(1)} = \frac{2N^3}{3} + 5N^2 + \frac{46}{3}N + 24UN - 24U - 15$	$C^{(2)} = 24UN + 15N - 2$	$C^{(3)} = 24U_RN + 15N - 2$	$C^{(4)} = 24U_{eR}N + 15N - 2$
Energy consumption in receiver-end processing, E_p			$\frac{C^{(1)}VI}{f}$	$\frac{C^{(2)}VI}{f}$	$\frac{C^{(3)}VI}{f}$	$\frac{C^{(4)}VI}{f}$

VI. Performance Results

The performance of the proposed methods was studied via MATLAB simulations. The wireless communication system as described in Section II was modeled with varying numbers of transmitters N and a single receiver. Each transmit signal was subject to additive white Gaussian noise (AWGN), a uniformly distributed phase shift to represent the initial phase offset of the transmitter's local oscillator, and a channel phase shift. The channel phase between each transmitter and the receiver was simulated by drawing random samples from a Nakagami-m phase distribution [35], with the severity of fading controlled by the parameter m. This approach allows for modeling different levels of fading severity. At the receiver, the proposed methods were applied to the phase impacted signals. The key performance metric for evaluation was the

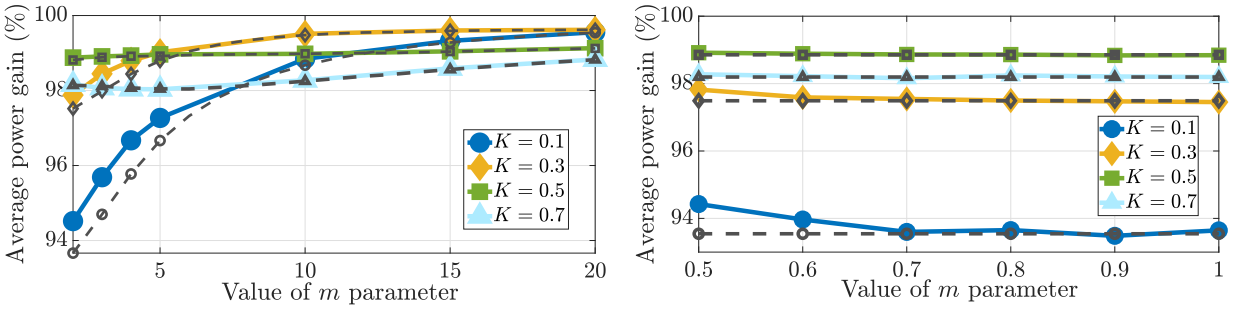

(a) $m > 1$ **(b)** $m \leq 1$

Fig. 4: Performance of extRSS for different values of K. $N = 2$. Solid line: simulation, dashed line: analysis.

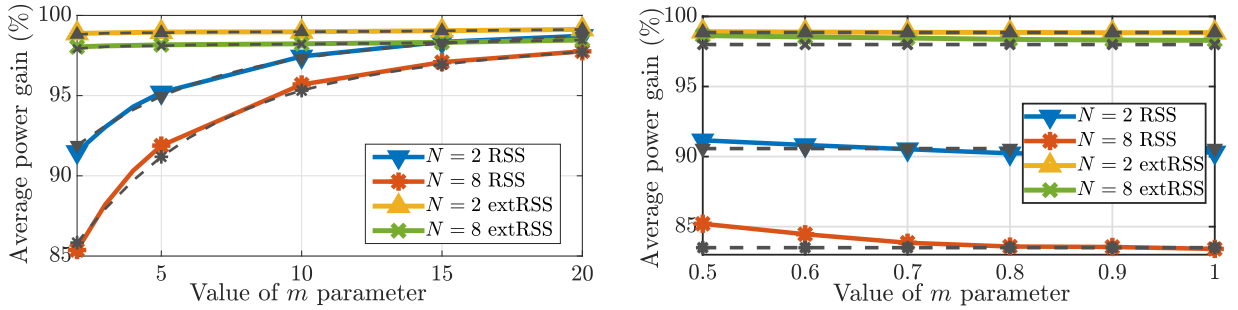

(a) $m > 1$ **(b)** m ≤ 1

Fig. 5: Power gain with RSS and extRSS methods for $K = 0.5$. Solid line: simulation, dashed line: analysis.

normalized power gain at the receiver as defined in Section II. This value was averaged over 1000+ iterations to ensure statistical reliability. The common system parameters considered are as follows: $f_c = 2.4$ GHz, $a_i = 1$, $A_i = 1$ V, and $\Delta = 0.1$ radian. Throughout the section, Nakagami-m fading channel is considered between each transmitter and the receiver. Further, $\phi_i \sim U[-\pi, \pi)$. AWGN with SNR $= 20$ dB is considered. These MATLAB simulations are also validated against numerical plots from the analytical formulations derived in Section V. In this section, the processing requirements and energy efficiency of the proposed methods are also evaluated. For this, a low-power wireless MCU based on Arm Cortex M4 is used as reference.

A. Performance of extRSS method for different K values

Fig. 4a shows the numerical and simulation results on average power gain achieved at the receiver using the extRSS method for different values of K for $m > 1$. It can be observed that while lower values of K provide higher gain for large values of m, there is a significant dip in power gain at low values of m, as the search points are clustered together, whereas the high probability areas are diffused. For $K = 0.5$, a stable gain of approximately 99% is achieved

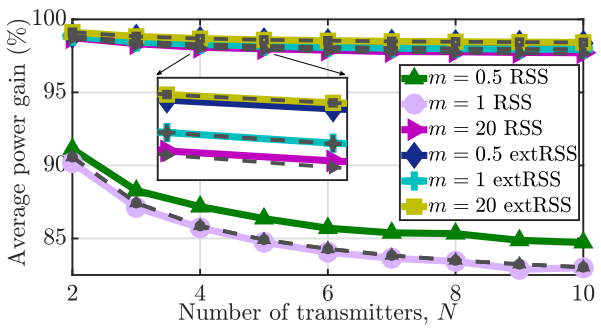

Fig. 6: Power gain vs. N. Simulation - RSS: solid line, extRSS ($K = 0.5$): dashed colored line. Analysis: grey.

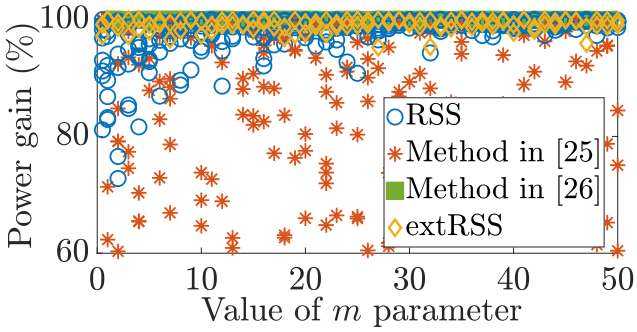

Fig. 7: Scatter plot on instantaneous power gain at the receiver as a function of m, for $K = 0.5$, $N = 2$.

for all values of m. If K is increased further, average power gain falls, as now the additional search points are very close to the low probability troughs and are not able to contribute to a significant power gain increase. Thus, $K = 0.5$ is able to achieve near-perfect average power gain independent of the severity of fading. Analytical plots corroborate the simulation results; the slight deviation for low values of m is due to the lower accuracy of the Gaussian mixture approximation (Proposition 2) for these values of m in the analysis.

For $m \leq 1$, the average power gain with extRSS method for different values of K (shown in Fig. 4b) has the same trend, with $K = 0.5$ providing a higher and stable gain across all values of $m \leq 1$. The small difference in numerical and simulation plots for lower values of m is due to the lower accuracy of the uniform distribution approximation (Proposition 3) in the analysis.

Remark 3. *Proposed extRSS method with $K = 0.5$ achieves near-perfect and fading agnostic average power gain at the receiver.*

B. Power gain with the proposed reduced search space methods

Fig. 5 shows the numerical and simulation results on average power gain versus m in the proposed RSS and extRSS methods with $K = 0.5$ for different values of N. The receiver achieves a near-perfect power gain in strong LOS conditions ($m \gg 1$) with the proposed RSS method. This performance demonstrates the applicability of the proposed RSS method for practical scenarios requiring energy-efficient collaborative transmissions, such as short-range communications, radiative wireless power transfer, or fixed backhaul communication links, where the LOS component can be dominant [27], [28]. As explained in Section IV, the RSS method is based on approximating the search space by exploiting the high probability areas of the channel phase distribution. Hence, there is a slight degradation in the achieved average power gain for

small values of m (weak LOS /non-LOS conditions), as the high probability areas are more diffused in this region. However, it can be noted that the proposed RSS method still works reasonably well. For $m \leq 1$, the performance is evaluated for the small range of permissible $0.5 \leq m \leq 1$ values. As the high probability areas are very diffused in this region (with the pdf $\rightarrow$ uniform distribution as shown in Proposition 3), the performance is slightly degraded here as well. As anticipated, the poorest performance is noted at $m = 1$ when the pdf is uniformly distributed and there are no high probability areas, with average power gain $> 80\%$. The proposed extRSS introduces 8 additional search points in the lower probability areas compared to RSS. This additional overhead compensates for the diffused high probability areas and achieves near-perfect average power gain at the receiver for all values of m, providing a complementary solution to the RSS method. Closely matched simulation results validate the analytical approximations.

The plots in Fig. 6 indicate that the average power gain at the receiver does not significantly reduce with N. In the RSS method, the gain saturates to $\frac{1}{N}P_N \rightarrow (\mathbb{E}[cos(X_i^{(n)})])^2$ as $N \rightarrow \infty$ [39], leading to an average power gain of 81.14% in the worst case of $m = 1$. The small reduction in gain is due to the accumulated de-synchronization errors as N increases. Significant improvement in average power gain in the proposed extRSS method is observed for large values of N as well. It may also be noted that the numerical plots for $m = 1$ and $m = 0.5$ exactly overlap, as the analytical expression for average power gain is independent of m for $m \leq 1$.

Fig. 7 shows the scatter plots of power gain in different methods under fast fading conditions with $N = 2$. The approach in [25] has significant gain variation under varying fading conditions, as it assumes slow fading channel for temporal extraction of signals across multiple time slots, and hence it is not fading-robust. The method in [26] achieves stable near-perfect gain; however, since it uses exhaustive search for high accuracy phase corrections, it is computationally intensive. In the RSS method, power gain has only minor variation for high values of m, i.e., with strong LOS. It has reduced computational overhead at the cost of approximation of the search space based on high probability areas. For low values of m, increased gain variation is observed, as the high probability areas are diffused. Thus, the RSS method is more suited in strong LOS conditions. In contrast, the extRSS method achieves near-perfect power gain at all values of m, at a marginally increased search overhead, thus showcasing its fading agnostic gain and channel tracking capability even under fast fading conditions. Thus, extRSS offers a complementary method that trades between computational complexity and phase alignment accuracy.

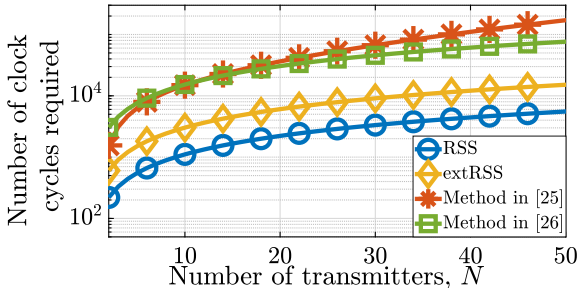

Fig. 8: Comparison of computational requirements in the proposed and competitive methods versus N.

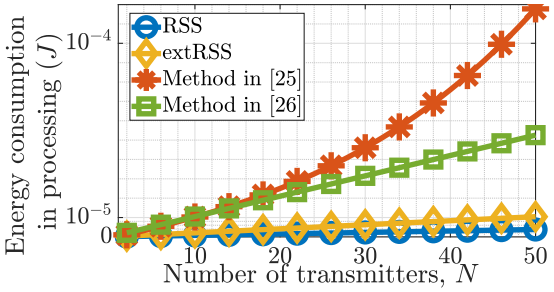

Fig. 9: Comparison of energy consumption in processing in the proposed and competitive methods.

Remark 4. *The receiver can seamlessly switch between the RSS and extRSS without any transmission overhead, based on the achieved power gain at the receiver under the prevailing fading conditions to balance between performance gain and energy consumption objectives.*

C. Processing requirement and energy consumption

Fig. 8 compares the processing overhead in executing the different competitive methods using the analysis summarized in Table I. The overhead is noted to be significantly reduced in the proposed methods compared to those in [25], [26]. The computational requirement is increased slightly in extRSS, though it is still much lower than the closest competitive methods. The processing energy consumption E_p is shown in Fig. 9. The plots demonstrate that the proposed methods are highly energy-efficient compared to the competitive approaches. The results further corroborate the scalability of the proposed methods, as the energy saving increases with N.

VII. Conclusion

This paper presented lightweight phase synchronization methods for resource-constrained nodes to achieve DBF-like received power gains. Power gain was achieved by using blind receiver-end phase estimation and correction, with only one transmission per transmitter. The receiver-end processing was vastly reduced by transforming the original N dimensional hypercube search space into N one-dimensional searches and then by exploiting the channel phase distribution characteristics to reduce the search space for each one-dimensional problem.

The proposed methods exploit the nonuniform Nakagami-m channel phase distribution to significantly reduce the phase correction search space, and they do not require the knowledge of m. They together provide energy-efficient phase synchronization in diverse fading conditions. It was

shown that in strong LOS conditions the RSS method with only 4 search points per transmitter is sufficient to achieve near-perfect power gain; even in weak LOS, the average power gain is above 80% of the ideal value. The extRSS method demonstrated fading severity agnostic near-perfect power gain with 12 search points per transmitter. These methods offer significantly reduced processing overhead compared to the closest competitive methods in the literature. They can enable practical deployments in energy-constrained wireless systems, including environmental monitoring, emergency communications, and distributed MIMO networks.

The future research directions include addressing the system non-idealities such as imperfect frequency and time synchronization, non-ideal orthogonality, and operation in low-SNR regimes.

APPENDIX

A. Proof of Proposition 1

Proof. Based on (4), (5) and the text below it, the receiver-end processing in the proposed phase synchronization problem requires solving the following optimization problem:

$$\textbf{(P1)} : \arg\max \left| \sum_{i=1}^{N} e^{j(\phi_i+\theta_i+\alpha_i)} \right|^2 \tag{A.1}$$
$$\text{s. t. } \textbf{(C1)} : 0 \leq \alpha_i < 2\pi \quad \forall i \in \{1, \cdots, N\}.$$

We consider the Cauchy-Schwarz inequality given by

$$\left| \sum_{i=1}^{N} e^{j(a_i-b_i)} \right|^2 \leq \sum_{i=1}^{N} \left| e^{j(a_i-b_i)} \right|^2 = N^2, \tag{A.2}$$

with the maximum value reached when $a_i = b_i \quad \forall i \in \{1, \cdots, N\}$. Hence, (A.1) is maximized when $\phi_i + \theta_i + \alpha_i = 0 \quad \forall i \in \{1, \cdots, N\}$. It can also be easily seen that the maximization holds even when $\phi_i + \theta_i + \alpha_i = \phi_0 \quad \forall i \in \{1, \cdots, N\}$ where ϕ_0 is an arbitrary phase, as

$$\text{LHS of (A.2)} = \left| \sum_{i=1}^{N} e^{j(a_i-b_i)} \right|^2 = \left| \sum_{i=1}^{N} e^{j\phi_0} \right|^2 = \left| e^{j\phi_0} \sum_{i=1}^{N} 1 \right|^2 = N^2. \tag{A.3}$$

□

B. Proof of Corollary to Proposition 1

Proof. From Proposition 1, we have $\left| \sum_{i=1}^{N} e^{j(\phi_i+\theta_i+\alpha_i)} \right|^2$, $0 \leq \alpha_i < 2\pi \quad \forall i \in \{1, \cdots, N\}$, which is maximized by $\phi_1 + \theta_1 + \alpha_1 = \phi_2 + \theta_2 + \alpha_2 = \cdots = \phi_N + \theta_N + \alpha_N$.

This can be generalized as $\left| \sum_{i=1}^{N} e^{j\Phi_i} \right|^2$, $0 \leq \alpha_i < 2\pi \quad \forall i \in \{1, \cdots, N\}$, and is maximized by $\Phi_1 = \Phi_2 = \cdots = \Phi_N$ where $\{\Phi_i\}$ may be any phase variables.

Let $N = 2$, $\Phi_1 = \phi_0$ and $\Phi_2 = \phi_i + \theta_i + \alpha_i$. Then, $\left|e^{j\phi_0} + e^{j(\phi_i+\theta_i+\alpha_i)}\right|^2$, $0 \leq \alpha_i < 2\pi \quad \forall i \in \{1, \cdots, N\}$ is maximized by $\phi_0 = \phi_i + \theta_i + \alpha_i$. Therefore, $\phi_i + \theta_i + \alpha_i = \phi_0$ is an optimal solution of $\left|e^{j\phi_0} + e^{j(\phi_i+\theta_i+\alpha_i)}\right|^2$, $0 \leq \alpha_i < 2\pi \quad \forall i \in \{1, \cdots, N\}$. □

C. Proof of Proposition 2

Proof. Consider the mathematical expression for Nakagami-m phase distribution,

$$p_\theta(\theta) = \frac{\Gamma(m)|sin(2\theta)|^{m-1}}{2^m\Gamma^2(\frac{m}{2})} = \mathcal{F}(m)|sin(2\theta)|^{m-1}, \quad \theta \in [-\pi, \pi) \tag{C.1}$$

where $\mathcal{F}(m) = \frac{\Gamma(m)}{2^m\Gamma^2(\frac{m}{2})}$. Dividing the domain into four segments and rewriting $p_\theta(\theta)$

$$= \mathcal{F}(m)\left[|\sin(2\theta)|^{m-1}\Big|_{\theta\in\left[-\pi,-\frac{\pi}{2}\right)} + |\sin(2\theta)|^{m-1}\Big|_{\theta\in\left[-\frac{\pi}{2},0\right)} + |\sin(2\theta)|^{m-1}\Big|_{\theta\in\left[0,\frac{\pi}{2}\right)} + |\sin(2\theta)|^{m-1}\Big|_{\theta\in\left[\frac{\pi}{2},\pi\right)}\right]$$

$$\begin{aligned}=\mathcal{F}(m)\Bigg[&\cos^{m-1}\left(2\theta + \frac{3\pi}{2}\right)\Big|_{\theta\in\left[-\pi,-\frac{\pi}{2}\right)} + \cos^{m-1}\left(2\theta + \frac{\pi}{2}\right)\Big|_{\theta\in\left[-\frac{\pi}{2},0\right)} \\ &+ \cos^{m-1}\left(2\theta - \frac{\pi}{2}\right)\Big|_{\theta\in\left[0,\frac{\pi}{2}\right)} + \cos^{m-1}\left(2\theta - \frac{3\pi}{2}\right)\Big|_{\theta\in\left[\frac{\pi}{2},\pi\right)}\Bigg].\end{aligned} \tag{C.2}$$

Here, the individual segments are written in terms of shifted cosine functions.

Now, consider the Taylor series expansion of $\cos^q x$,

$$\cos^q x = 1 - q\frac{x^2}{2!} + q(3q-2)\frac{x^4}{4!} - q(15q^2 - 30q + 16)\frac{x^6}{6!} + \cdots. \tag{C.3}$$

For large values of q, (C.3) can be simplified as

$$\cos^q x = 1 - \frac{qx^2}{2} + \frac{q^2x^4}{8} - \frac{q^3x^6}{48} + \cdots. \tag{C.4}$$

Also, consider the Taylor series expansion of $e^{-\frac{qx^2}{2}}$,

$$e^{-\frac{qx^2}{2}} = 1 - \frac{q}{1!}\frac{x^2}{2} + \frac{q^2}{2!}\frac{x^4}{4} - \frac{q^3}{3!}\frac{x^6}{8} + \cdots. \tag{C.5}$$

Hence, comparing (C.4) and (C.5) and neglecting the higher order terms we have

$$(\cos^q x)\Big|_{x\in\left[-\frac{\pi}{2},\frac{\pi}{2}\right]} \approx e^{-\frac{qx^2}{2}}. \tag{C.6}$$

Fig. C.1 shows fitness of approximation in (C.6) for power of cosine function, even for small q.

Substituting suitably shifted versions of (C.6) in (C.2) and solving, with $\sigma^2 = \frac{1}{4(m-1)}$, we have

$$p_\theta(\theta) \approx \mathcal{F}(m)\left[e^{-2(m-1)\left(\theta+\frac{3\pi}{4}\right)^2} + e^{-2(m-1)\left(\theta+\frac{\pi}{4}\right)^2} + e^{-2(m-1)\left(\theta-\frac{\pi}{4}\right)^2} + e^{-2(m-1)\left(\theta-\frac{3\pi}{4}\right)^2}\right] \tag{C.7}$$

$$= \mathcal{K}(m)\left[\mathcal{N}\left(-\frac{3\pi}{4}, \sigma^2\right) + \mathcal{N}\left(-\frac{\pi}{4}, \sigma^2\right) + \mathcal{N}\left(\frac{\pi}{4}, \sigma^2\right) + \mathcal{N}\left(\frac{3\pi}{4}, \sigma^2\right)\right] \tag{C.8}$$

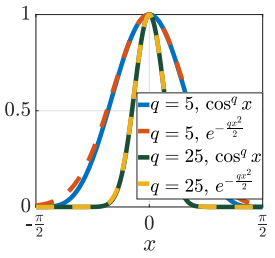

Fig. C.1: Exponential approximation for cosine.

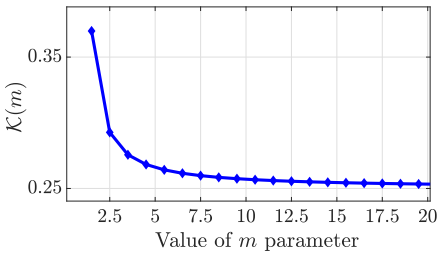

Fig. C.2: $\mathcal{K}(m)$ plotted for different values of m using (C.9).

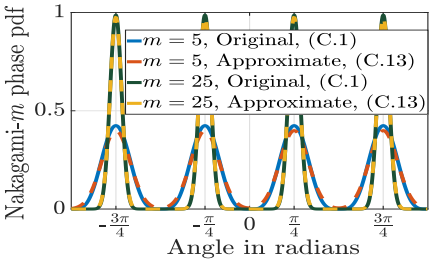

Fig. C.3: Efficacy of the Gaussian mixture approximation.

$$\mathcal{K}(m) = \mathcal{F}(m) \times \sqrt{2\pi\sigma^2} = \frac{\Gamma(m)}{2^m \Gamma^2(\frac{m}{2})} \sqrt{\frac{2\pi}{4(m-1)}}. \tag{C.9}$$

Using $\Gamma(n) = (n-1)!$ for non-negative integers, we have,

$$\mathcal{K}(m) = \frac{(m-1)!}{2^m (\frac{m}{2}-1)!\,(\frac{m}{2}-1)!} \sqrt{\frac{2\pi}{4(m-1)}} \tag{C.10}$$

Applying the Stirling formula given by $n! \approx \sqrt{2\pi n}(\frac{n}{e})^n$ and simplifying,

$$\mathcal{K}(m) = \frac{\sqrt{2\pi(m-1)}(\frac{m-1}{e})^{(m-1)}}{2^m \times 2\pi(\frac{m}{2}-1)\left(\frac{\frac{m}{2}-1}{e}\right)^{2(\frac{m}{2}-1)}} \sqrt{\frac{2\pi}{4(m-1)}} \tag{C.11}$$

$$= \frac{(\frac{m-1}{e})^{(m-1)}}{2^{m+1}(\frac{m}{2}-1)\left(\frac{\frac{m}{2}-1}{e}\right)^{(m-2)}} = \frac{(\frac{m-1}{e})^{(m-1)}}{2^{m+1}(\frac{m-2}{2})\left(\frac{m-2}{2e}\right)^{(m-2)}} = \frac{(\frac{m-1}{e})^{(m-1)}}{4(m-2)\left(\frac{m-2}{e}\right)^{(m-2)}} \tag{C.12}$$

Multiplying and dividing by $\sqrt{2\pi(m-1)}$ and $\sqrt{2\pi(m-2)}$, we have,

$$\mathcal{K}(m) = \frac{\sqrt{2\pi(m-1)}(\frac{m-1}{e})^{(m-1)}}{4\sqrt{(m-1)(m-2)}\sqrt{2\pi(m-2)}\left(\frac{m-2}{e}\right)^{(m-2)}} \tag{C.13}$$

Using the Stirling formula, this is simplified to

$$\mathcal{K}(m) = \frac{1}{4\sqrt{(m-1)(m-2)}} \frac{(m-1)!}{(m-2)!} = \frac{1}{4}\sqrt{\frac{m-1}{m-2}} \tag{C.14}$$

It is notable from (C.14) that for large integer values of m, $\mathcal{K}(m) \to \frac{1}{4}$. The trend holds for non-integer values as well as confirmed from the plot in Fig. C.2. This is also indeed the requirement to make this approximation of $p_\theta(\theta)$ a valid pdf. Hence, for large values of m, we have,

$$p_\theta(\theta) \approx \frac{1}{4}\left[\mathcal{N}\left(\frac{-3\pi}{4}, \sigma^2\right) + \mathcal{N}\left(\frac{-\pi}{4}, \sigma^2\right) + \mathcal{N}\left(\frac{\pi}{4}, \sigma^2\right) + \mathcal{N}\left(\frac{3\pi}{4}, \sigma^2\right)\right]. \tag{C.15}$$

The plots in Fig. C.3 indicate that Gaussian mixture approximation (C.15) is a good match for the Nakagami-m phase pdf (C.1), even for comparatively smaller values of m. □

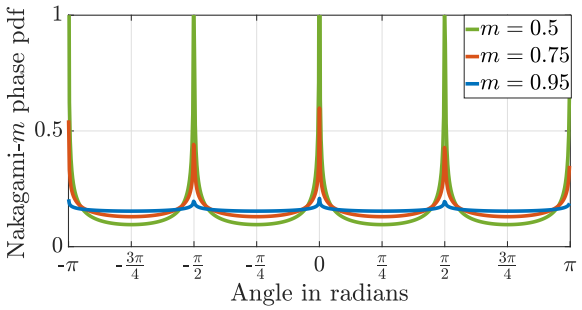

Fig. D.1: Nakagami-m phase pdf for $m \leq 1$.

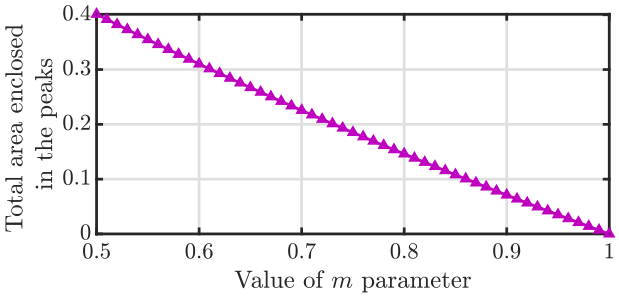

Fig. D.2: Total probability of the four peaks for $m \leq 1$.

D. Proof of Proposition 3

Proof. To prove the uniform distribution approximation of Nakagami-m distribution for $m \leq 1$, we need to show that the area enclosed by the peak regions is negligible for $m \to 1^-$.

Consider the interval $[0, \frac{\pi}{2})$ which covers one peak of the Nakagami-m phase distribution in $[-\pi, \pi)$ when $m \leq 1$. As can be seen from Fig. D.1, the Nakagami-m phase distribution is symmetric about 0 and $\frac{\pi}{2}$, as $p_\theta(-\theta) = p_\theta(\theta)$ and $p_\theta(\pi/2+\theta) = p_\theta(\pi/2-\theta)$ respectively where, $p_\theta(\theta)$ is defined in (10), hence, the total area (probability) under $f(\theta)$ for $\theta \in [0, \frac{\pi}{2})$ is $\frac{1}{4}$.

Now, consider the minimum point of $f(\theta)$, occurring at $\theta = \frac{\pi}{4}$ (using first derivative of $f(\theta)$):

$$f(\theta)\Big|_{\theta=\frac{\pi}{4}} = \frac{\Gamma(m)}{2^m \Gamma^2(\frac{m}{2})}. \tag{D.1}$$

The area A_{peak} enclosed in a peak is approximated as the area under the curve $f(\theta)$ minus the rectangular area in $\theta \in [0, \frac{\pi}{2})$ below $f(\theta)\Big|_{\theta=\frac{\pi}{4}}$. Thus, $A_{peak} = \frac{1}{4} - \frac{\pi}{2} \times f(\theta)\Big|_{\theta=\frac{\pi}{4}}$ is found as

$$A_{peak} = \frac{1}{4} - \frac{\pi\Gamma(m)}{2^{m+1}\Gamma^2(\frac{m}{2})} \tag{D.2}$$

Fig. D.2 shows the plot of total area (probability) enclosed in the four peaks for $m \leq 1$ based on (D.2). It can be observed that, despite the impulse-like appearance of the peaks, the area enclosed by the peaks is insignificant when the value of m is close to 1. Thus, uniform distribution is a reasonably accurate approximation of Nakagami-m phase pdf for $m \to 1^-$. □

REFERENCES

[1] Y. Shi and Y. E. Sagduyu, "Coherent communications in self-organizing networks with distributed beamforming," *IEEE Trans. Veh. Technol.*, vol. 69, no. 1, pp. 760–770, 2020.

[2] S. Jayaprakasam, S. K. A. Rahim, and C. Y. Leow, "Distributed and collaborative beamforming in wireless sensor networks: Classifications, trends, and research directions," *IEEE Commun. Surveys Tuts.*, vol. 19, no. 4, pp. 2092–2116, 2017.

[3] D. Mishra and S. De, "Optimal relay placement in two-hop RF energy transfer," *IEEE Trans. Commun.*, vol. 63, no. 5, pp. 1635–1647, 2015.

[4] K. W. Choi, A. A. Aziz, D. Setiawan, N. M. Tran, L. Ginting, and D. I. Kim, "Distributed wireless power transfer system for Internet of Things devices," *IEEE Internet Things J*, vol. 5, no. 4, pp. 2657–2671, 2018.

[5] T. D. Ponnimbaduge Perera, D. N. K. Jayakody, S. K. Sharma, S. Chatzinotas, and J. Li, "Simultaneous wireless information and power transfer (SWIPT): Recent advances and future challenges," *IEEE Commun. Surveys Tuts.*, vol. 20, no. 1, pp. 264–302, 2018.

[6] R. G. Cid-Fuentes, M. Y. Naderi, S. Basagni, K. R. Chowdhury, A. Cabellos-Aparicio, and E. Alarcón, "On signaling power: Communications over wireless energy," in *Proc. IEEE INFOCOM*, 2016, pp. 1–9.

[7] R. Mudumbai, B. J. Wild, U. Madhow, and K. Ramchandran, "Distributed beamforming using 1 bit feedback : From concept to realization," in *Proc. Allerton Conf. Commun. Control Comput.*, 2006.

[8] R. Mudumbai, D. R. Brown III, U. Madhow, and H. V. Poor, "Distributed transmit beamforming: challenges and recent progress," *IEEE Commun. Mag.*, vol. 47, no. 2, pp. 102–110, 2009.

[9] I. Thibault, A. Faridi, G. E. Corazza, A. V. Coralli, and A. Lozano, "Design and analysis of deterministic distributed beamforming algorithms in the presence of noise," *IEEE Trans. Commun.*, vol. 61, no. 4, pp. 1595–1607, 2013.

[10] D. Richard Brown, P. Bidigare, and U. Madhow, "Receiver-coordinated distributed transmit beamforming with kinematic tracking," in *Proc. IEEE ICASSP*, 2012, pp. 5209–5212.

[11] R. Wang, R. David, and D. R. Brown, "Feedback rate optimization in receiver-coordinated distributed transmit beamforming for wireless power transfer," in *Proc. Annual Conf. Inform. Sci. Syst.*, 2015, pp. 1–6.

[12] D. Bharadia and S. Katti, "FastForward: Fast and constructive full duplex relays," *Proc. ACM SIGCOMM*, pp. 199–210, 2014.

[13] Q. Wang and K. Ren, "Time-slotted round-trip carrier synchronization in large-scale wireless networks," in *Proc. IEEE ICC*, 2008, pp. 5087–5091.

[14] S. Lee and R. Zhang, "Distributed energy beamforming with one-bit feedback," in *Proc. IEEE WCNC*, 2016, pp. 398–403.

[15] S. R. Mghabghab and J. A. Nanzer, "Open-loop distributed beamforming using wireless frequency synchronization," *IEEE Trans. Microw. Theory Techn.*, vol. 69, no. 1, pp. 896–905, 2021.

[16] K. Alemdar, D. Varshey, S. Mohanti, U. Muncuk, and K. R. Chowdhury, "RFClock: Timing, phase and frequency synchronization for distributed wireless networks," in *Proc. ACM MobiCom*, 2021, pp. 15–27.

[17] A. Muralidharan and Y. Mostofi, "Energy optimal distributed beamforming using unmanned vehicles," *IEEE Control Netw. Syst*, vol. 5, no. 4, pp. 1529–1540, 2018.

[18] X. Xu, X. Chen, M. Zhao, S. Zhou, C. Chi, and J. Wang, "Power-efficient distributed beamforming for full-duplex MIMO relaying networks," *IEEE Trans. Veh. Technol.*, vol. 66, no. 2, pp. 1087–1103, 2017.

[19] R. Wang and D. R. Brown, "Optimal wireless power transfer with distributed transmit beamforming," *J. Commun. Netw.*, vol. 19, no. 2, pp. 134–146, 2017.

[20] Z. Lin, Y. Gong, and K. Huang, "Distributed over-the-air computing for fast distributed optimization: Beamforming design and convergence analysis," *IEEE Journal on Selected Areas in Communications*, vol. 41, no. 1, pp. 274–287, Jan. 2023.

[21] A. Bhattacharyya and J. A. Nanzer, "Multiobjective distributed beamforming using high-accuracy synchronization and localization," *IEEE Transactions on Microwave Theory and Techniques*, vol. 72, no. 4, pp. 1497–1508, Apr. 2024.

[22] A. Mittal, A. Sinha, S. K. Kaul, and S. Srinivasan, "An ultralow-power closed-loop distributed beamforming technique for efficient wireless power transfer," *IEEE Internet of Things Journal*, vol. 11, no. 19, pp. 9065–9077, Oct. 2024.

[23] K. D. Nguyen, G. Lechner, and I. Ahmad, "Zero-feedback open-loop distributed transmit beamforming," *Digital Signal Processing*, vol. 156, p. 104875, 2025.

[24] A. Bletsas, A. Lippman, and J. N. Sahalos, "Simple, zero-feedback, collaborative beamforming for emergency radio," in *Proc. IEEE Int. Symp. Wireless Commun. Syst.*, 2009, pp. 657–661.

[25] M. U. P. Sriploy, "Nonfeedback distributed beamforming using spatial-temporal extraction," *Int. J. Antennas Propag.*, vol. 2016, pp. 1–16, 2016.

[26] S. Sachdev and S. De, "Energy efficient receiver-end distributed beamforming using orthogonal transmissions," *IEEE Commun. Lett.*, vol. 26, no. 7, pp. 1648–1652, 2022.

[27] D. Mishra, S. De, S. Jana, S. Basagni, K. Chowdhury, and W. Heinzelman, "Smart RF energy harvesting communications: Challenges and opportunities," *IEEE Commun. Mag.*, vol. 53, no. 4, pp. 70–78, 2015.

[28] D. Mishra and S. De, "Utility maximization models for two-hop energy relaying in practical RF harvesting networks," in *Proc. IEEE ICC*, 2017, pp. 41–46.

[29] M. Nakagami, "The m-distribution – A general formula of intensity distribution of rapid fading," in *Statistical Methods in Radio Wave Propagation*, W. Hoffman, Ed. Pergamon, 1960, pp. 3–36.

[30] C. Polprasert and J. A. Ritcey, "A nakagami fading phase difference distribution and its impact on BER performance," *IEEE Trans. Wireless Commun.*, vol. 7, no. 7, pp. 2805–2813, 2008.

[31] H. A. Suraweera, D. S. Michalopoulos, and C. Yuen, "Performance analysis of fixed gain relay systems with a single interferer in Nakagami- m fading channels," *IEEE Trans. Veh. Technol.*, vol. 61, no. 3, pp. 1457–1463, 2012.

[32] M. Hafez, T. Khattab, and H. M. H. Shalaby, "Blind SNR estimation of gaussian-distributed signals in Nakagami fading channels," *IEEE Trans. Wireless Commun.*, vol. 14, no. 7, pp. 3509–3518, 2015.

[33] F. Louzada, P. L. Ramos, and D. Nascimento, "The inverse Nakagami-m distribution: A novel approach in reliability," *IEEE Trans. Reliability*, vol. 67, no. 3, pp. 1030–1042, 2018.

[34] R. C. Ferreira, M. S. P. Facina, F. A. P. De Figueiredo, G. Fraidenraich, and E. R. De Lima, "Bit error probability for large intelligent surfaces under double-Nakagami fading channels," *IEEE Open J. Commun. Soc.*, vol. 1, pp. 750–759, 2020.

[35] M. D. Yacoub, G. Fraidenraich, and J. C. S. Santos Filho, "Nakagami-m phase-envelope joint distribution," *Electron. Lett.*, vol. 41, no. 5, pp. 259–261, 2005.

[36] M. D. Yacoub, "Nakagami-m phase–envelope joint distribution: A new model," *IEEE Trans. Veh. Technol.*, vol. 59, no. 3, pp. 1552–1557, 2010.

[37] R. K. Mallik, "A new statistical model of the complex Nakagami-m fading gain," *IEEE Trans. Commun.*, vol. 58, no. 9, pp. 2611–2620, 2010.

[38] I. B. G. Porto, M. D. Yacoub, J. C. S. Santos Filho, S. L. Cotton, and W. G. Scanlon, "Nakagami-m phase model: Further results and validation," *IEEE Wireless Commun. Lett.*, vol. 2, no. 5, pp. 523–526, 2013.

[39] R. Mudumbai, G. Barriac, and U. Madhow, "On the feasibility of distributed beamforming in wireless networks," *IEEE Trans. Wireless Commun.*, vol. 6, no. 5, pp. 1754–1763, 2007.

[40] J. C. Silveira Santos Filho and M. D. Yacoub, "On the simulation and correlation properties of phase-envelope Nakagami fading processes," *IEEE Trans. Commun.*, vol. 57, no. 4, pp. 906–909, 2009.

[41] D. B. da Costa, M. D. Yacoub, J. C. S. S. Filho, G. Fraidenraich, and J. R. Mendes, "Generalized Nakagami-m phase crossing rate," *IEEE Commun. Lett.*, vol. 10, no. 1, pp. 13–15, 2006.

[42] "Cortex-m4 technical reference manual r0p0: Fpu instruction set," https://developer.arm.com/documentation/ddi0439/b/BEHJADED, accessed: 2022-06-19.